Generalized least-squares DSR migration using a common angle imaging condition

Henning Kuehl and Mauricio D. Sacchi, University of Alberta

Summary

Pre-stack wave equation migration based on generalized phase-shift operators can generate accurate depth images in complex geological environments. In (generalized) DSR (Double-Square-Root) migration the complete pre-stack dataset is processed simultaneously. The standard imaging condition for DSR migration extracts the zero time wavefield at zero offset, resulting in a single depth image. A common angle imaging (CAI) condition can be employed that extracts the zero time wavefield for a set of constant offset ray parameters. The CAI gathers provide amplitude versus angle (AVA) information and are suitable for residual velocity analysis. Furthermore, CAI gathers are an attractive domain for the regularization least-squares (LS) migration.

One can regularize the inverse problem by imposing a smooth solution along the ray parameter domain. This is similar to offset smoothing in Kirchhoff LS migration. The regularization penalizes discontinuities that can be attributed to imaging artifacts and footprint noise. A tradeoff parameter is used to control the degree of smoothing in order to preserve amplitude with angle variations and residual velocity moveout.

Introduction

Least-squares (LS) migration based on Kirchhoff modeling/migration operators has been proposed in the literature to account for uneven subsurface illumination and to mitigate imaging artifacts due to irregularly and coarsely sampled seismic wavefields (Nemeth et al., 1999; Duquet et al., 2000). Duquet et al. (2000) demonstrate how to further improve the LS migration results by applying a smoothing constraint along the offset domain in the common reflection point (CRP) gathers. In Kuehl and Sacchi (2001) we show that, in principle, the concept of LS migration can also be applied to phase-shift DSR (Double-Square-Root) migration (Claerbout, 1985) by introducing a data covariance matrix.

However, as in LS Kirchhoff migration additional regularization of the inverse problem is desirable. Mosher and Foster (2000) proposed a common angle imaging (CAI) condition for wave equation based wavefield extrapolators that provides the equivalent of migrated tau-p gathers for each CMP location (Ottolini, 1984). The CAI condition in conjunction with generalized DSR wavefield extrapolators (e.g. split-step DSR operator (Popovici, 1996)) is cast in a least-squares migration framework with a smoothing constraint along the ray parameter domain. The additional constraint penalizes discontinuities that can be attributed to numerical imaging artifacts and footprint noise.

Theory

Wavefield propagators for LS pre-stack depth migration

Inverse scattering theory provides an instructive framework for deriving phase-shift WKBJ DSR modeling and migration operators (Stolt and Benson, 1986). These operators are valid for vertically varying background (migration) velocities. Various approaches exist to generalize the operators for velocity variations perpendicular to the direction of wave propagation by appropriate expansion of the square-root terms (Claerbout, 1985). Here we focus on two such operators, the split-step DSR and the split-step DSR operator using multiple reference velocities. 0ther more accurate techniques exist (e.g. Ristow and Rühl, 1994; Grimbergen et al , 1998).

Split-step DSR migration is based on the following approximation of the square root terms in the DSR operator (Stoffa et al., 1990):

$$\sqrt{\frac{\omega^2}{c^2(x,z)}-k^2}=\sqrt{\frac{\omega^2}{c^2(z)}-k^2}+\left(\frac{\omega}{c(x,z)}-\frac{\omega}{c(z)}\right), \tag{1}$$

where $c(x,z)$ is the background (migration) velocity, $c(z)$ is the inverse of the average lateral slowness at each depth level, and ω is the angular frequency. The k^2 term is the horizontal wavenumber of either the source or the receiver position (Popovici, 1996). Applying this approximation to the DSR operator yields a recursive downward wavefield propagrator that can be symbolically written as:

$$\psi(z+dz)=\mathbf{F}\,\mathbf{S}\,\mathbf{F}^{-1}\,\mathbf{DSR}\,\psi(z), \tag{2}$$

where **DSR** is the propagator using the reference velocity $c(z)$ applied to the wavefield in the midpoint-offset wavenumber domain. **S** represents the split-step correction term in the midpoint-offset space domain. The symbols **F** and $\mathbf{F}^{-1}$ are forward and inverse midpoint-offset Fourier transforms, respectively. To perform least-squares migration the adjoint upward wavefield propagator needs to be known:

$$\tilde{\psi}(z)=\mathbf{DSR}'\,\mathbf{F}\,\mathbf{S}'\,\mathbf{F}^{-1}\psi(z+dz), \tag{3}$$

with the prime denoting the adjoint form of an operator. The DSR operator can be further generalized by introducing the logic of multiple reference velocities. This can be particularly important in DSR modeling and migration because, unlike shot migration, the DSR operator processes all midpoints simultaneously. The DSR propagator is factorized into a receiver and a source propagator: $\mathbf{DSR} = \mathbf{P}_s\,\mathbf{P}_r$. We define a wavefield copying and linear wavefield interpolation operator **C** and $\mathbf{I}_r$, respectively. The initial pre-stack data is Fourier transformed over time, midpoint, and offset. The first operator creates N identical copies of the wavefield, where N is the number of chosen reference velocities. After propagating the

reference wavefields by the receiver operator $\mathbf{P_r}$ the split-step operator **S** is applied with respect to the reference velocities. Next the interpolation $\mathbf{I_r}$ of the wavefields is carried out in midpoint-offset space according to the actual (laterally varying) velocities at the receiver positions. After Fourier transforming the interpolated result back to the midpoint-offset wavenumber domain the same procedure is repeated for the sources. This results in a cascaded PSPI (split-step) DSR downward propagator that can be symbolically expressed as follows:

$$\psi(z+dz) = \mathbf{F\, I_s\, S_s\, F^{-1}\, P_s\, C\, F\, I_r\, S_r\, F^{-1}\, P_r\, C}\psi(z). \qquad (4)$$

We note that the split-step correction was introduced implicitly by Gazdag and Squazzero (1984) into their PSPI algorithm to assure an accurate propagation of vertically travelling plane waves. Again, upon interchanging the order of the operators and taking their individual adjoint forms we find the PSPI DSR upward propagator:

$$\tilde{\psi}(z) = \mathbf{C'\, P'_r\, F\, S'_r\, I'_r\, F^{-1}\, C'\, P'_s\, F\, S'_s\, I'_s\, F^{-1}}\psi(z+dz). \qquad (5)$$

This corresponds to the windowed Non-Stationary-Phase-Shift (NSPS) operator described by Margrave and Ferguson (1999) extended by the adjoint of interpolation and the split-step correction and applied to DSR upward propagation.

The common angle imaging condition

Mosher and Foster (2000) suggest a common angle imaging (CAI) condition for pre-stack depth migration. The summation over frequency and offset wavenumber for the standard imaging condition of DSR migration is replaced with multiple summations over the offset ray parameter $p=k_h/\omega$. In two dimensions this amounts to summing along radial lines in the (k_h,ω) domain with slope p. Rather than a single image at each depth step, multiple images are produced, one for each offset ray parameter. We denote the CAI imaging operator by **A**. The operator **A** extracts the images (the model) at each depth step *dz* from the downward propagated wavefield:

$$m_p = \mathbf{A}\psi, \qquad (6)$$

where m_p constitutes a set of constant ray parameters images. In modeling, the adjoint operator $\mathbf{A'}$ feeds the images m_p back into the wavefield at each depth,

$$\tilde{\psi} = \mathbf{A'}m_p, \qquad (7)$$

followed by upward propagation with step size *dz*. Depending on the complexity of the background velocity either the split-step DSR or the PSPI DSR propagator is used for downward/upward wavefield propagation.

Least-squares migration with ray parameter smoothing

The modeling/migration operator pair is used to invert the linear system:

$$d = \mathbf{L}\, m_p + n, \qquad (8)$$

where *d* is the binned data (noisy and incomplete), **L** the modeling operator (combining the propagator and the adjoint of the CAI condition) and m_p the set of constant ray parameter images or the model. The error term *n* represents modeling errors, missing data and noise. We minimize the following objective function using a conjugate gradient (CG) algorithm:

$$\mathrm{F(m)} = \| \mathbf{W}(\mathrm{d} - \mathbf{A}\mathrm{m}) \|_2 + \lambda \sum_p \| m_p - m_{p-1} \|_2, \qquad (9)$$

where **W** is a (diagonal) weighting operator with zero weights for dead traces and non-zero weights for live traces according to their noise level. The scaling factor λ is a tradeoff parameter. The second term in the objective function imposes a relative smoothing constraint that suppresses undesired discontinuities (imaging artifacts and footprint noise) in the ray parameter direction. The tradeoff parameter serves to control the amount of smoothing.

Examples

We illustrate LS DSR migration with ray parameter smoothing using the Marmousi dataset. Figure 1A shows the CAI gather at CMP 175 of a total of 240 CMPs. The gathers were produced with offset ray parameters in the range from 0 to 760 µsec/m incrementing by 40 µsec/m. The processing time for the migration of the 240 CMPs was about 50 s on an SGI 2400 using 32 processors. AVA effects, residual velocity errors and numerical imaging artifacts are apparent. We note that for reliable AVA analysis obliquity factors must be included that are introduced by the implied Radon transform over offset (Mosher and Foster, 1998). To test the influence of missing data on the imaging result we randomly replaced 80% of the shots by dead traces prior to migration. The CAI panel in Figure1B illustrates the effect of footprint noise. The image exhibits stronger incoherent noise and the continuity along the ray parameter domain is further deteriorated. However, given that 80% of the data is missing the general robustness of DSR migration is remarkable. The effect of LS migration with 1% of offset smoothing is demonstrated in Figure 1C. The CAI gather was obtained after 3 iterations of the CG algorithm. The LS algorithm has partially restored the continuity along the ray parameter axis and improved the signal to noise ratio. After 6 iterations the smoothing effect is more pronounced and the energy is more smeared along p (Figure 1D). In Figure 1E the velocity profile at CMP 175 is depicted for comparison.

The Figures 2A/B and 2C/D illustrate the effect of missing data and the benefits of LS migration for images generated using a single constant p (160 µsec/m), respectively. The quality of the LS migrated images has clearly improved.

In Figure 3 it is demonstrated that this improvement of the separate p gathers does not necessarily imply an improved stacked image. The healing power of stacking has essentially the same effect on the final stack as the offset smoothing term.

Discussion and Conclusion

Generalized LS DSR migration using a common angle imaging condition allows to incorporate a regularization by ray parameter smoothing. The logic behind ray parameter

smoothing is based on the idea that discontinuities along the ray parameter axis stem from numerical imaging artifacts and missing data. The smoothing regularization term is controlled by a tradeoff parameter. Care must be taken to preserve amplitude variation with angle effects and residual velocity moveout when migration velocity analysis is performed. Criteria for the appropriate degree of smoothing and the effects on the reliability of amplitude versus angle variations have to be studied in more detail in the future.

Acknowledgements

We would like to acknowledge the following companies and organizations: PanCanadian, Geo-X, Schlumberger Foundation, Veritas Geoservices, NSERC and Alberta Department of Energy. We would also like to thank Dr. Biondi for his discussion on DSR migration.

References

Claerbout, J.F., 1985, Imaging the Earth's Interior, Blackwell Scientific Publications.

Duquet, B., Marfurt, J.K., and Dellinger, J.A., 2000, Kirchhoff modeling, inversion for reflectivity, and subsurface illumination, Geophysics, **65**, 1195-1209.

Gazdag, J., and Squazzero, P., 1984, Migration of seismic data by phase shift plus interpolation, Geophysics, **49**, 124-131.

Grimbergen, J.L.T, Dessing, F.J., and Wapenaar, K., 1998, Modal expansion of one-way operators in laterally varying media, Geophysics, **63**, 995-1005.

Kuehl, H., and Sacchi, D.M., 2001, Split-step WKBJ least-squares migration/inversion of incomplete data, 5th SEGJ International Symposium – Imaging Technology.

Margrave, G.F., and Ferguson, R.J., 1999, Wavefield extrapolation by nonstationary phase shift, Geophysics, **64**, 1067-1078.

Mosher, C.C., and Foster, D.J., 2000, Common angle imaging conditions for pre-stack depth migration, 70th Annual Internat. Mtg., Soc. Expl. Geophys., Expanded Abstracts, MIG 4.4.

Mosher, C.C., and Foster, D.J., 1998, Offset plane wave propagation in laterally varying media, in Mathematical Methods in Geophysical Imaging V, S. Hassanzadeh, ed., Proc. SPIE 3453, 36-46.

Nemeth, T., Wu, C., and Schuster, G.T., 1999, Least-squares migration of incomplete reflection data, Geophysics, **64**, 208-221.

Ottolini, R., and Claerbout, J.F., 1984, The migration of common midpoint slant stacks, Geophysics, **49**, 237-249.

Popovici, A.M., 1996, Prestack migration by split-step DSR, Geophysics, **59**, 1412-1416.

Ristow, D., and Rühl, T., 1994, Fourier finite-difference migration, Geophysics, **59,** 1882-1893.

Stoffa, P.L., Fokkema, J.T.. de Luna Freire, R.M., and Kessinger, W.P., 1990, Split-step migration, Geophysics, **55,** 410-421.

Stolt, R.H., and Benson, A.K., 1986, Seismic Migration: Theory and Practice, Geophysical Press.

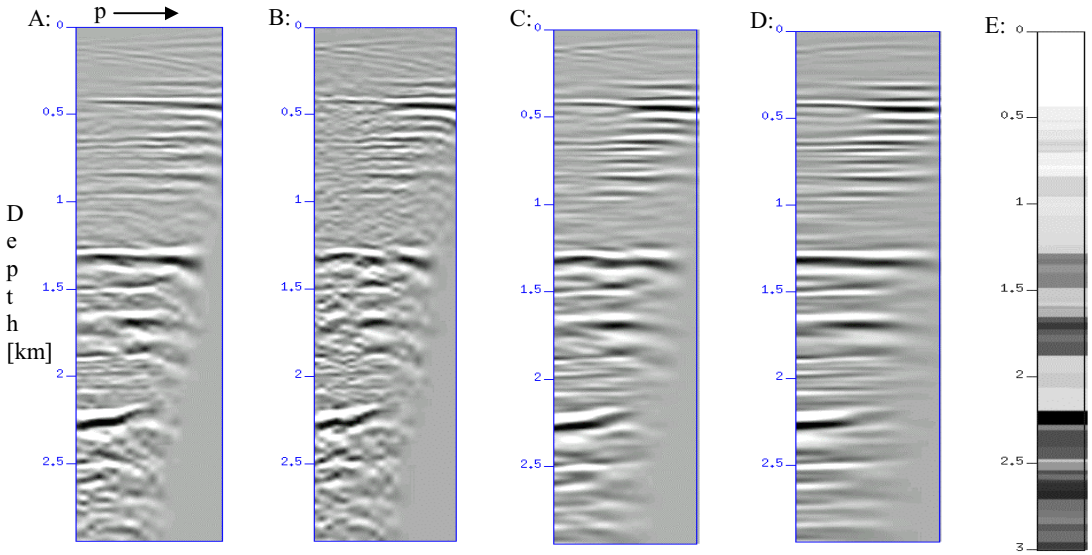

Figure1: CAI gathers and velocity profile of CMP 175 of the Marmousi dataset. A: The CAI gather of the complete Marmousi dataset. B: CAI gather of the reduced dataset. About 80% of the shots have been randomly removed. C: The same CMP after 3 iterations of the CG algorithm with 1% smoothing. D: Result after 6 iterations using the same tradeoff parameter as in C. E: The velocity profile at CMP 175.

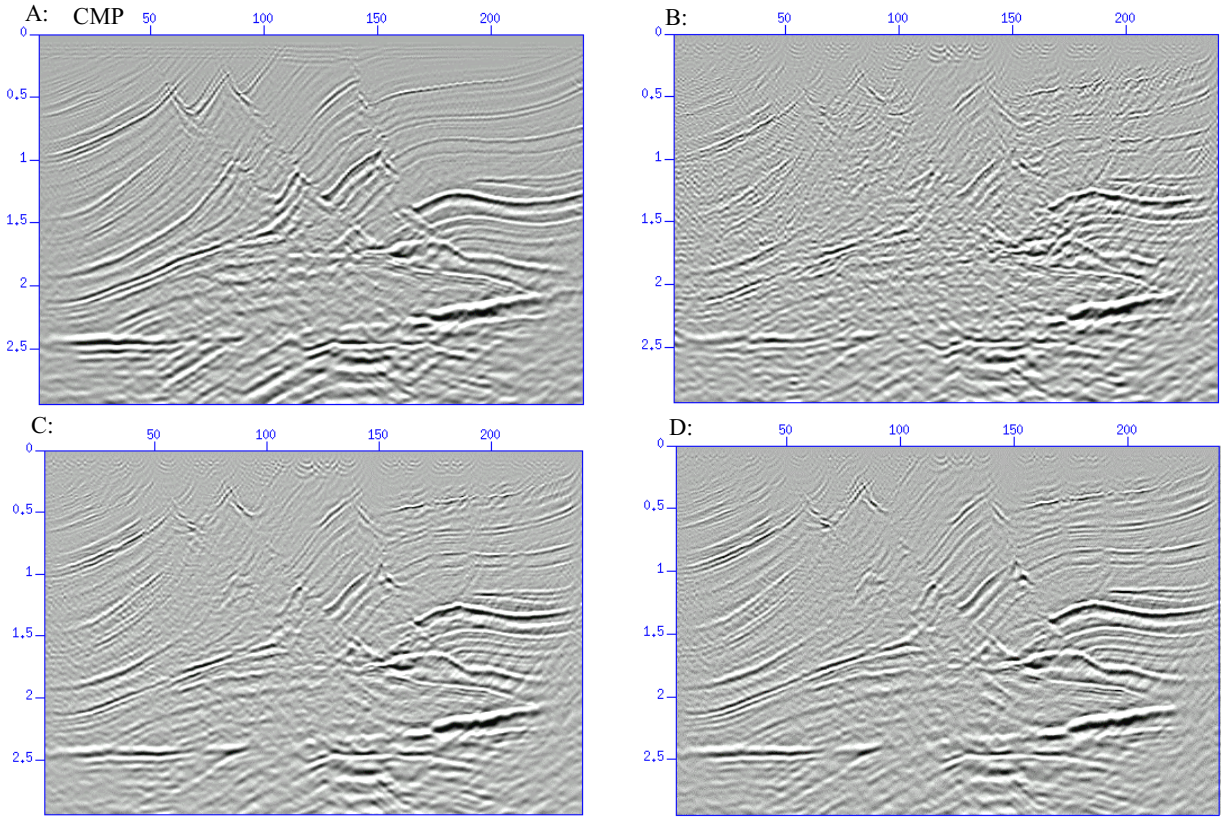

Figure 2: CAI images with a constant offset ray parameter of 160 μsec/m. A: Constant offset ray parameter migration of the complete dataset. B: Constant offset ray parameter migration of the incomplete dataset (80% of the shots are set to zero). C: LS migration with ray parameter smoothing of the incomplete data after 3 iterations of the CG algorithm. D: Result after 6 iterations of the CG algorithm.

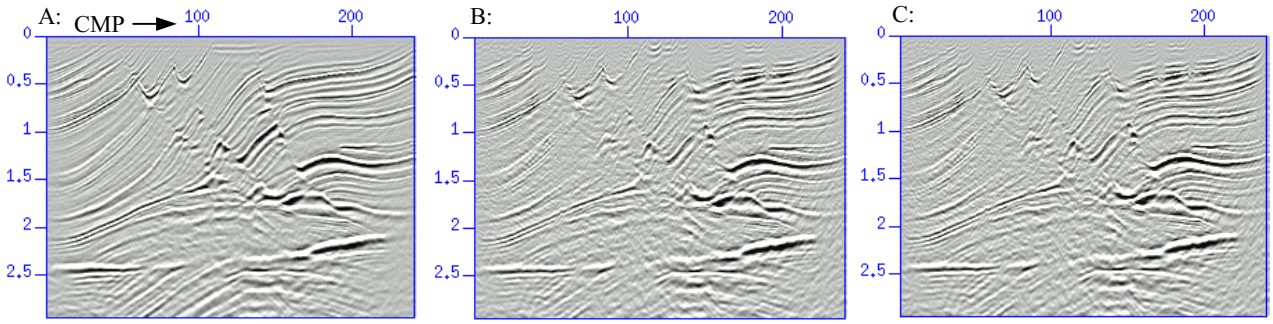

Figure 3: A: The stacked CAI gathers of the complete dataset. B and C show the stacked migration and the stacked LS migration (6 iterations with ray parameter smoothing) of the reduced dataset, respectively. Note the robustness of DSR migration with respect to missing data. The conventional migration and the LS migrated images (B and C) are almost identical. This can be explained by the tremendous healing effect of stacking.